Electronic Supplementary Material (ESI) for New Journal of Chemistry.

ELECTRONIC SUPPLEMENTARY MATERIAL

Supramolecular Inter-Ionic Charge-Transfer Complexes Between Deriviatives of Pyridinium-4-oxime Cations and Hexacyanoferrate(II) Anion

Blaženka Foretić,*[a] Robert Vianello, [b] Dubravka Matković-Čalogović,[c] Dijana Jadreško [d] and Igor Picek*[a]

[a]*Department of Chemistry and Biochemistry, School of Medicine, University of Zagreb, Šalata 3, HR-10000 Zagreb, Croatia*

[b]*Division of Organic Chemistry and Biochemistry, Ruđer Bošković Institute, Bijenička 54, HR-10000 Zagreb, Croatia*

[c]*Department of Chemistry, Faculty of Science, University of Zagreb, Horvatovac 102a, HR-10000 Zagreb, Croatia*

[d]*Division for Marine and Environmental Research, Ruđer Bošković Institute, Bijenička 54, HR-10000 Zagreb, Croatia*

Corresponding author's contact information:

E-mail: ipicek@mef.hr

E-mail: bforetic@mef.hr

CYCLIC VOLTAMMETRY (*E* in V vs. Ag/AgCl (3M KCl))

		E_p / V			
		PAM4-I	BPA4-Cl	TMB4-2Br	TOXO-2Cl
Oxidation	A1	– 0.262	– 0.230	– 0.267	– 0.255
	A2	0.563	0.596	0.619	0.617
Reduction	C1	– 0.114	– 0.062	– 0.350	– 0.252
	C2	– 0.839	– 0.770	– 0.772	– 0.692
	C3	– 1.113	– 1.026	– 1.114	– 0.975
	C4	– 1.549	– 1.457	– 1.458	– 1.571

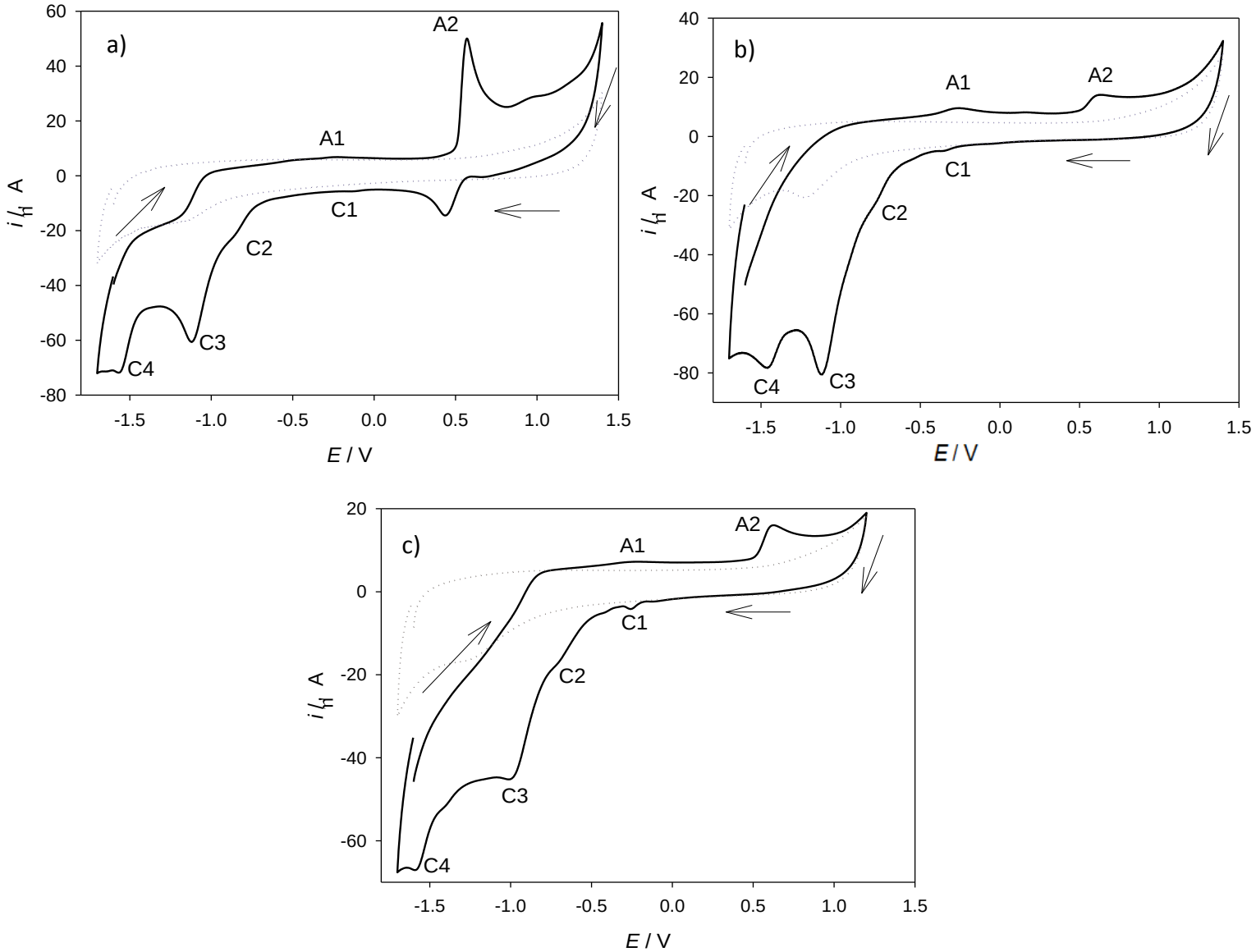

Fig. S1 Cyclic voltammogram (–) of a) 1 mM PAM4-I solution b) 0.76 mM TMB4-2Br solution and c) 0.76 mM TOXO-2Cl solution on glassy carbon electrode (···) in 0.1 M $NaClO_4$. A scan rate, *v* = 100 mV/s. Arrows indicate the scan direction. *E* in V vs. Ag/AgCl (3M KCl).

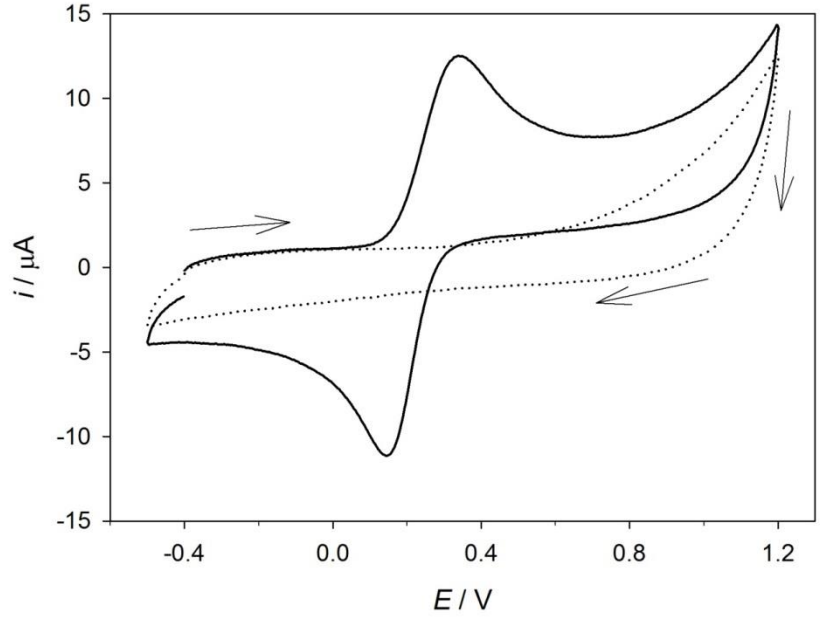

Fig. S2 Cyclic voltammogram (–) of 1 mM $K_4[Fe(CN)_6]$ solution on glassy carbon electrode in (···) 0.1 M $NaClO_4$. A scan rate, *v* = 100 mV/s. Arrows indicate the scan direction.

UV/Vis absorption properties and correlations

Determination of the equilibrium association constants (K_{ass}/M^{-1}) for the inter-ionic charge-transfer complex formation and corresponding molar absorption coefficients ($\varepsilon_{maxCT}/M^{-1}\ cm^{-1}$)

Solutions contained 3.0 – 12 mM of mono-pyridinium-4-oxime ($PAM4^{+}$, $BPA4^{+}$) or 0.5 –2.0 mM of bis-piridinium-4-oxime ($TMB4^{2+}$, $TOXO^{2+}$) and donor ($[Fe^{II}(CN)_6]^{4-}$) to maintain a IICT complex stoichiometry of 1:1. All solutions were of pH 5.35-5.88 and the ionic strength was adjusted using sodium chloride as inert electrolyte. The spectrophotometric runs of the thermally equilibrated solution contained in a cuvette were started immediately (25 °C). The electronic absorption spectrum of such solution represents the sum of all absorbing components in the solution. The time-dependent spectrum collection have shown that within around 10 minutes after reactant mixing the absorption band maximum is exclusively associated with the CT state of the formed IICT complex, which is the only species to have an appreciable absorbance. The maximal absorbance value, after longer exposition, is primarily influenced by the formation of the $[Fe^{III}(CN)_6]^{3-}$ which absorbs Vis light at 420 nm (ε=1040 $M^{-1}cm^{-1}$), while $[Fe^{II}(CN)_6]^{4-}$ as donor has negligible absorption. Furthermore, the pH-dependent absorption spectra of the investigated mono- and bis-pyridinium-4-oxime cations, previously characterized in detail (see ref. 11 and 12) revealed negligible absorption in the visible range at the pH range specified above. Therefore, the IICT band intensity is used to obtain the equilibrium association constant (K_{ass}/M^{-1}) and corresponding molar absorption coefficient ($\varepsilon_{maxCT}/M^{-1}\ cm^{-1}$) for the 1:1 dyad, assuming the formation of the neutral $A/K_3[Fe^{II}(CN)_6]$ or $A/K_2[Fe^{II}(CN)_6]$ IICT complexes. Namely, for the given concentration range the influence of the high negative charge in hexacyanoferrate(II) on its stability must be taken into account. This is based on a recent publication in which a hybrid QM/MM-MD simulations and extended X-ray absorption fine structure (EXAFS) experiments demonstrated that the $[Fe^{II}(CN)_6]^{4-}$ is stabile only in the presence of potassium counterions *i.e.* as $K_4[Fe^{II}(CN)_6]$ (see ref 32b).

a)

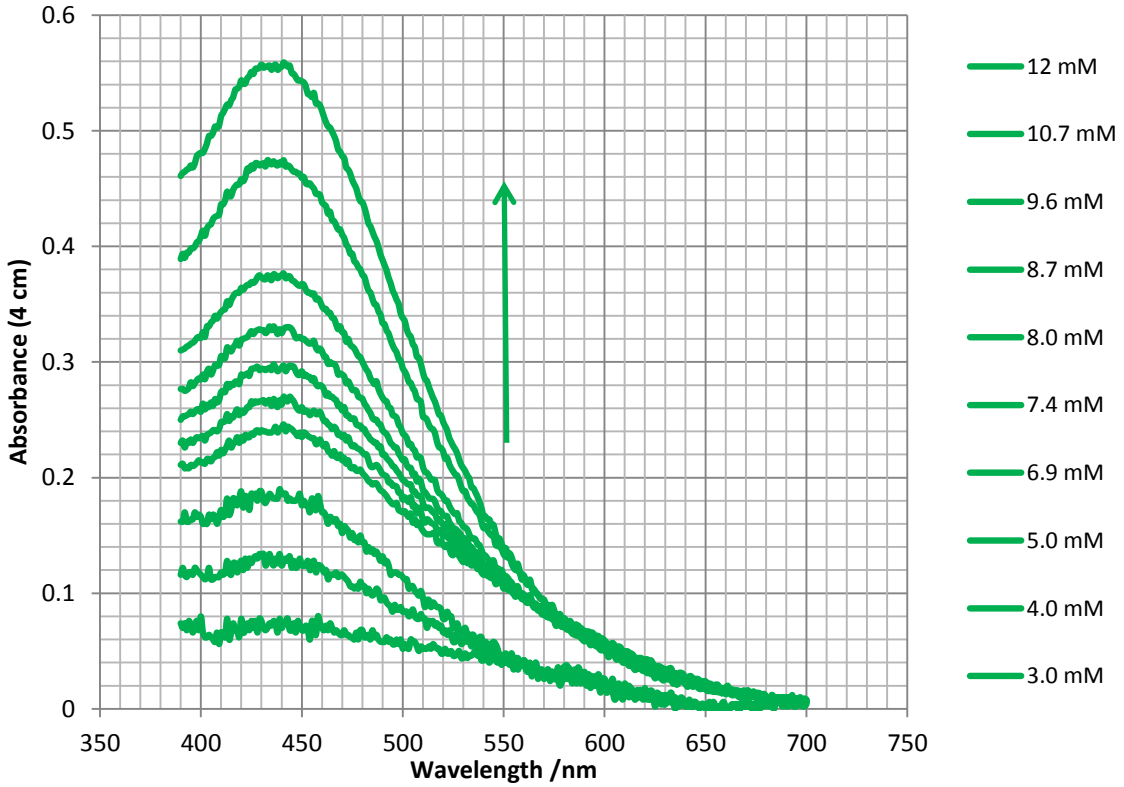
Absorbance (4 cm)
0.6
0.5
0.4
0.3
0.2
0.1
0
350
400
450
500
550
600
650
700
750
Wavelength /nm
12 mM
10.7 mM
9.6 mM
8.7 mM
8.0 mM
7.4 mM
6.9 mM
5.0 mM
4.0 mM
3.0 mM

b)

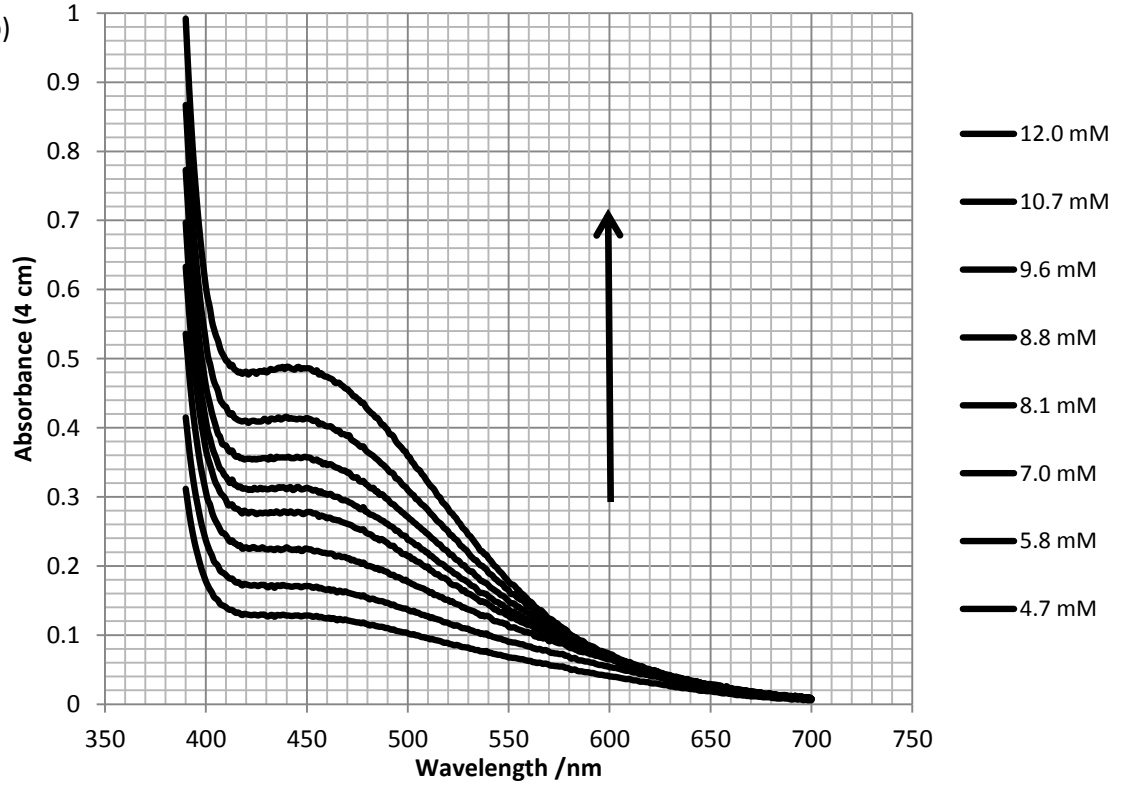
Absorbance (4 cm)
1
0.9
0.8
0.7
0.6
0.5
0.4
0.3
0.2
0.1
0
350
400
450
500
550
600
650
700
750
Wavelength /nm
12.0 mM
10.7 mM
9.6 mM
8.8 mM
8.1 mM
7.0 mM
5.8 mM
4.7 mM

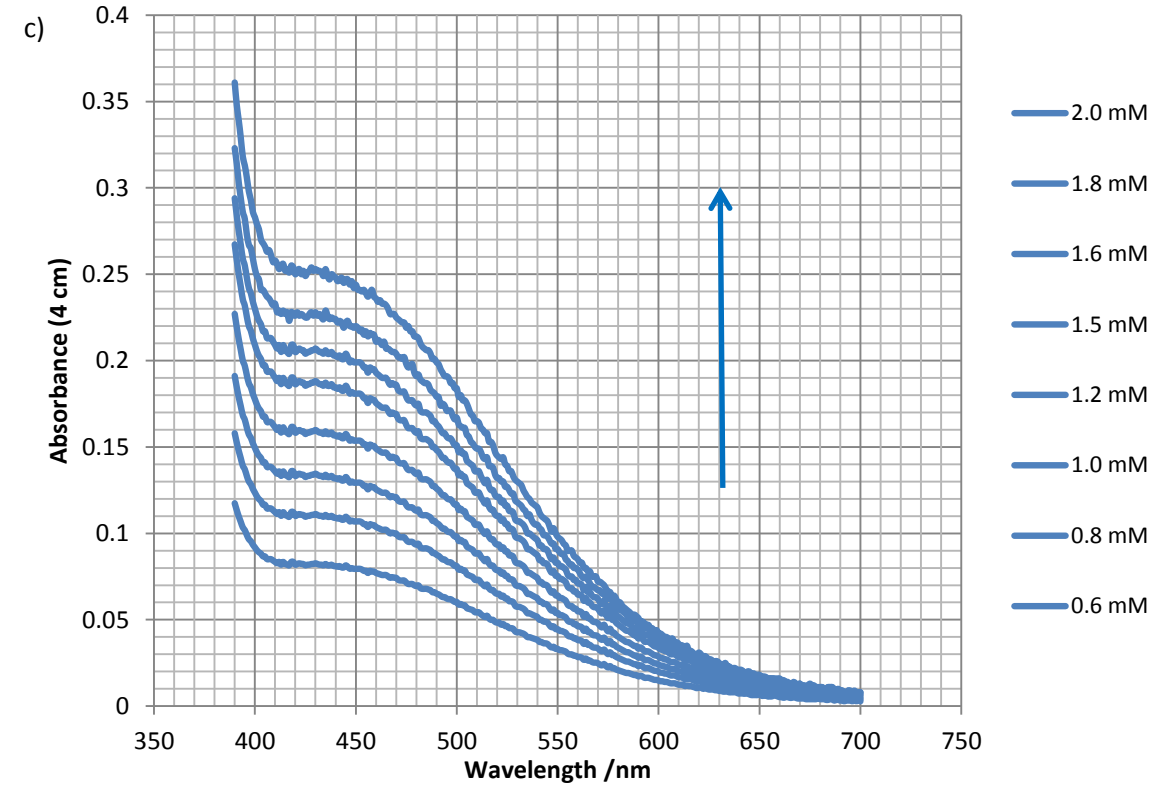

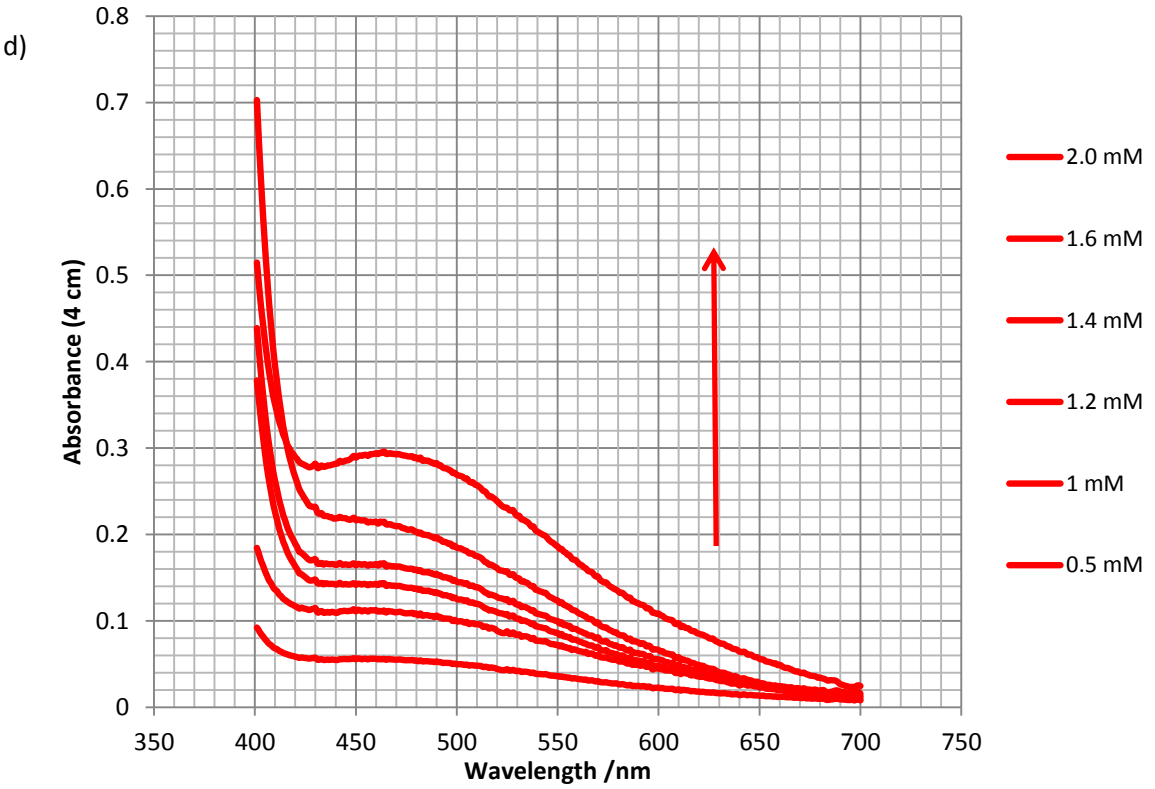

Fig. S3 Absorption spectra of the aqueous IICT complexes formed between $[Fe^{II}(CN)_6]^{4-}$ and: a) $PAM4^+$, b) $BPA4^+$, c) $TMB4^{2+}$and d) $TOXO^{2+}$. Reactants were present at different equimolar concentrations at pH = 5.65 ± 0.25, *t* = (25.1 ± 0.1) °C and *I* = 0.12 M.

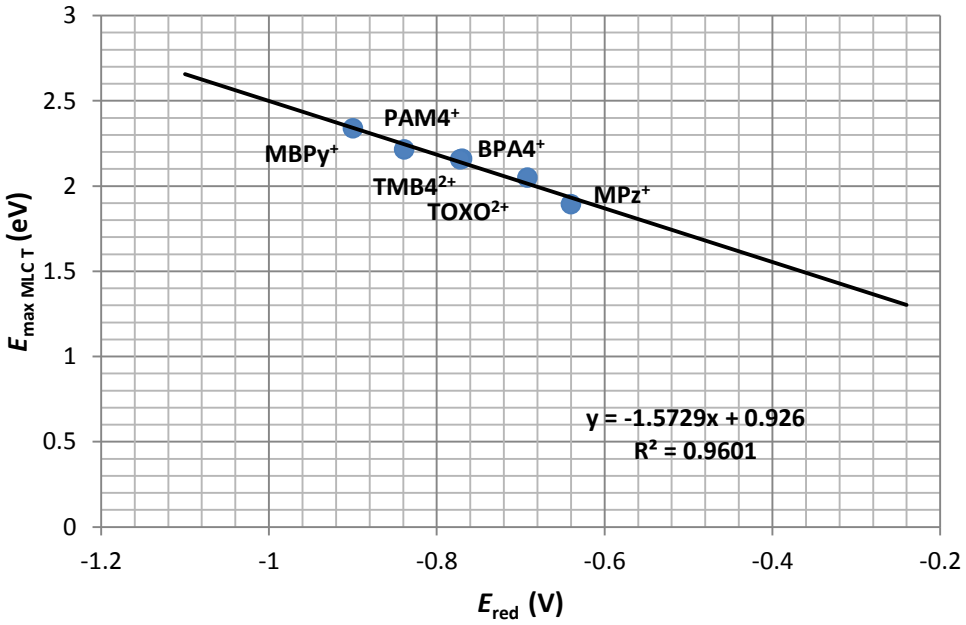

Fig. S4 Mulliken correlation between the transition energies of the visible range MLCT band for pentacyano(ligand) ferrate(II) complexes and the ligands' one-electron reduction potentials. The pyridinium-4-oxime, bipyridinium and pyrazinium derivatives as accepting ligands are presented.[11,16]

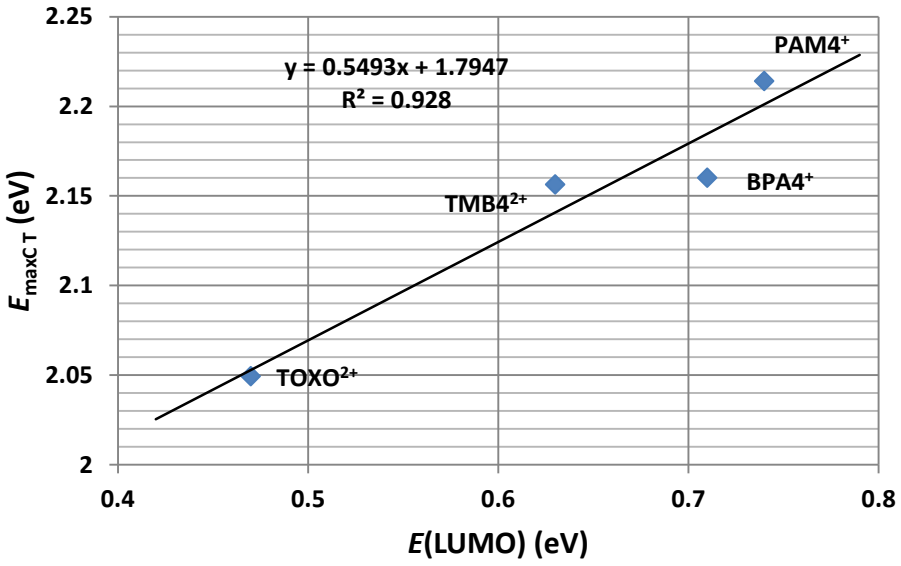

Fig. S4a A plot showing the linear correlation between IICT energies of mono-pyridinium-4-oxime^{+}/$[Fe^{II}(CN)_6]^{4-}$ and bis-pyridinium-4-oxime^{2+}/$[Fe^{II}(CN)_6]^{4-}$ complexes and the calculated LUMO energies of the corresponding pyridinium-4-oxime.

Calculation details in aqueous media

Table S1 Calculated solvation energies, electron affinities and reduction potentials.

$L^{n+} + e^- \text{-----> } L^{\bullet n+}$

SYSTEM	E_A(gas phase)	$\Delta G_{SOLV}(L^{\bullet n+})$	$\Delta G_{SOLV}(L)$	$\Delta\Delta G_{SOLV}$	$E_{Asolution}$ ($E_{A\ gas\ phase}$ - $\Delta\Delta G_{SOLV}$)	$E_{calcd\ solution}$ (vs Ag/AgCl; 3M KCl)
PAM4$^+$	-124.4 kcal/mol -5.39 eV	-11.0 kcal/mol -0.48 eV	-56.4 kcal/mol -2.45 eV	45.4 kcal/mol 1.97 eV	-79.1 kcal/mol **-3.43 eV**	**– 0.98 V**
BPA4$^+$	-122.3 kcal/mol -5.30 eV	-12.3 kcal/mol -0.53 eV	-54.2 kcal/mol -2.35 eV	41.9 kcal/mol 1.82 eV	-80.4 kcal/mol **-3.49 eV**	**– 0.92 V**
TMB4^{2+}	-175.0 kcal/mol -7.59 eV	-68.8 kcal/mol -2.98 eV	-162.5 kcal/mol -7.05 eV	93.8 kcal/mol 4.07 eV	-81.3 kcal/mol **-3.53 eV**	**– 0.88 V**
TOXO^{2+}	-180.6 kcal/mol -7.83 eV	-68.9 kcal/mol -2.99 eV	-163.9 kcal/mol -7.11 eV	95.1 kcal/mol 4.12 eV	-85.5 kcal/mol **-3.71 eV**	**– 0.70 V**

E(solution) = E_A(gas phase) - $\Delta\Delta G_{SOLV}$ – E(reference; solution)

E_A(solution) = E_A(gas phase) - $\Delta\Delta G_{SOLV}$

Absolute electrode potential:

$E^M_{(abs)} = E^M$(vs SHE) + $E^{SHE}_{(abs)}$

$E^{SHE}_{(abs;\ solution)} = 4.2 \pm 0.4$ V;[S1]

$E^M_{(abs)}$ (Ag/AgCl; solution) = E(Ag/AgCl; 3M KCl) $_{vs\ SHE}$ - E_{abs}(SHE solution) = 0.21 V + 4.20 V = 4.41 V.

S1. W. A. Donald, R. D. Leib, J. T. O'Brien, M. F. Bush and E. R. Williams, *J. Am. Chem. Soc.*, 2008, **130**, 3371–3381.

^{1}H NMR spectroscopic studies

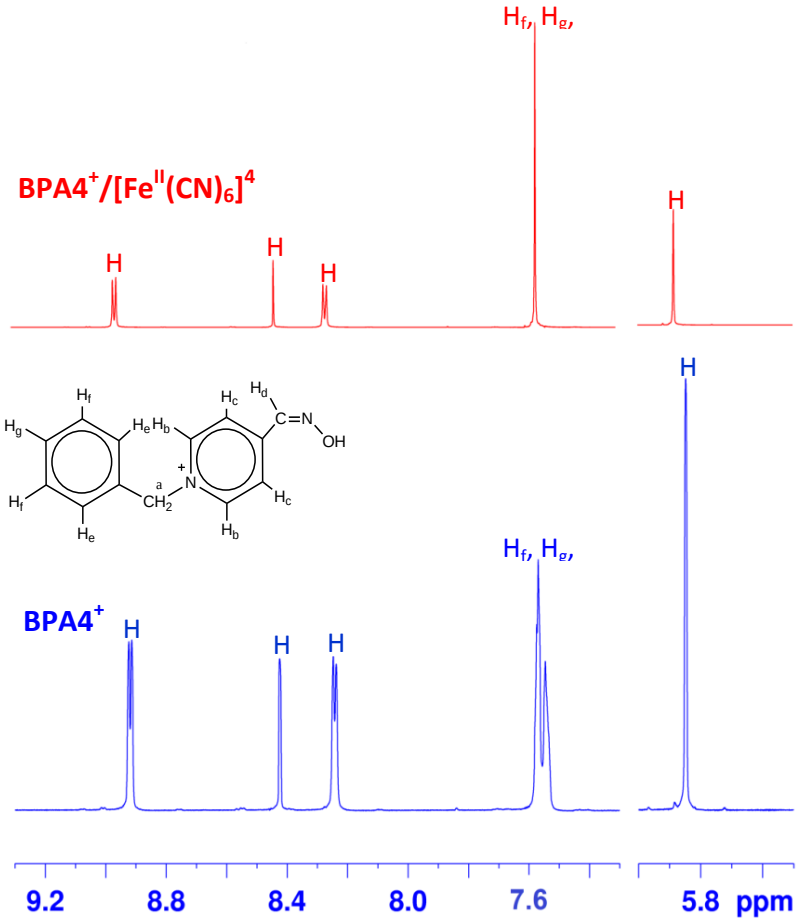

Fig. S5 ^{1}H-NMR spectra of (red) and BPA4$^+$/ $[Fe^{II}(CN)_6]^{4-}$ (blue) in D_2O at 25 °C; *c*(BPA4-Cl) = *c*($[Fe^{II}(CN)_6]^{4-}$) = 25 mM. The ^{1}H-NMR spectra were calibrated by using residual undeuterated solvent as an internal reference (4.80 ppm).

Table S2 ^{1}H-NMR chemical shifts observed for A^{+} and $A^{+}/[Fe^{II}(CN)_6]^{4-}$system in D_2O at room temperature.

$A^{+} \equiv PAM4^{+}$

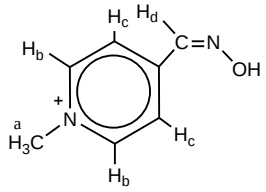

15 mM $PAM4^{+}$			15 mM $PAM4^{+}/[Fe^{II}(CN)_6]^{4-}$			$(\delta_{obs}-\delta_{PAM4})$/ppm	$(\delta_{obs}-\delta_{PAM4})$/Hz[c]
H_{PAM4}	δ_{PAM4}/ppm[a]	J/Hz	H_{PAM4}	δ_{obs}/ppm[b]	J/Hz		
H_a	4.417	–	H_a	4.458	–	0.041	24.61
H_b	8.803	6.78	H_b	8.849	6.60	0.046	27.61
H_c	8.228	6.78	H_c	8.249	6.54	0.021	12.60
H_d	8.432	–	H_d	8.442	–	0.010	6.00
25 mM $PAM4^{+}$			25 mM $PAM4^{+}/[Fe^{II}(CN)_6]^{4-}$			$(\delta_{obs}-\delta_{PAM4})$/ppm	$(\delta_{obs}-\delta_{PAM4})$/Hz[c]
H_{PAM4}	δ_{PAM4}/ppm[a]	J/Hz	H_{PAM4}	δ_{obs}/ppm[b]	J/Hz		
H_a	4.415	–	H_a	4.466	–	0.051	30.61
H_b	8.802	6.78	H_b	8.858	6.78	0.056	33.61
H_c	8.225	6.72	H_c	8.253	6.72	0.028	16.80
H_d	8.429	–	H_d	8.444	–	0.015	9.00
35 mM $PAM4^{+}$			35 mM $PAM4^{+}/[Fe^{II}(CN)_6]^{4-}$			$(\delta_{obs}-\delta_{PAM4})$/ppm	$(\delta_{obs}-\delta_{PAM4})$/Hz[c]
H_{PAM4}	δ_{PAM4}/ppm[a]	J/Hz	H_{PAM4}	δ_{obs}/ppm[b]	J/Hz		
H_a	4.419	–	H_a	4.478	–	0.059	35.41
H_b	8.806	6.66	H_b	8.871	6.72	0.065	39.01
H_c	8.228	6.66	H_c	8.262	6.72	0.034	20.40
H_d	8.432	–	H_d	8.450	–	0.018	10.80
45 mM $PAM4^{+}$			45 mM $PAM4^{+}/[Fe^{II}(CN)_6]^{4-}$			$(\delta_{obs}-\delta_{PAM4})$/ppm	$(\delta_{obs}-\delta_{PAM4})$/Hz[c]
H_{PAM4}	δ_{PAM4}/ppm[a]	J/Hz	H_{PAM4}	δ_{obs}/ppm[b]	J/Hz		
H_a	4.420	–	H_a	4.490	–	0.070	42.01
H_b	8.807	6.66	H_b	8.884	6.72	0.077	46.21
H_c	8.229	6.60	H_c	8.270	6.72	0.041	24.61
H_d	8.432	–	H_d	8.455	–	0.023	13.80
65 mM $PAM4^{+}$			65 mM $PAM4^{+}/[Fe^{II}(CN)_6]^{4-}$			$(\delta_{obs}-\delta_{PAM4})$/ppm	$(\delta_{obs}-\delta_{PAM4})$/Hz[c]
H_{PAM4}	δ_{PAM4}/ppm[a]	J/Hz	H_{PAM4}	δ_{obs}/ppm[b]	J/Hz		
H_a	4.426	–	H_a	4.505	–	0.079	47.41
H_b	8.813	6.60	H_b	8.901	6.72	0.088	52.81
H_c	8.234	6.48	H_c	8.281	6.66	0.047	28.21
H_d	8.436	–	H_d	8.463	–	0.027	16.20

$A^+ \equiv BPA4^+$

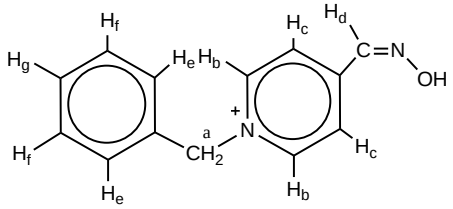

15 mM $BPA4^+$			15 mM $BPA4^+/[Fe^{II}(CN)_6]^{4-}$			$(\delta_{obs} - \delta_{BPA4})$/ppm	$(\delta_{obs} - \delta_{BPA4})$/Hz[c]
H_{BPA4}	δ_{BPA4}/ppm[a]	J/Hz	H_{BPA4}	δ_{obs}/ppm[b]	J/Hz		
H_a	5.854	-	H_a	5.890	-	0.036	21.60
H_b	8.924	6.90	H_b	8.960	5.64	0.036	21.60
H_c	8.250	6.84	H_c	8.272	5.64	0.022	13.20
H_d	8.431	-	H_d	8.446	-	0.015	9.00
H_e	multiplicity 7.549 – 7.585		H_e	one broad signal 7.566		-	-
H_f			H_f			-	-
H_g			H_g			-	-

25 mM $BPA4^+$			25 mM $BPA4^+/[Fe^{II}(CN)_6]^{4-}$			$(\delta_{obs} - \delta_{BPA4})$/ppm	$(\delta_{obs} - \delta_{BPA4})$/Hz[c]
H_{BPA4}	δ_{BPA4}/ppm[a]	J/Hz	H_{BPA4}	δ_{obs}/ppm[b]	J/Hz		
H_a	5.848	-	H_a	5.885	-	0.037	22.20
H_b	8.919	5.82	H_b	8.958	6.84	0.039	23.41
H_c	8.242	5.82	H_c	8.270	6.78	0.028	16.80
H_d	8.428	-	H_d	8.440	-	0.012	7.20
H_e	multiplicity 7.546 – 7.574		H_e	one broad signal 7.566		-	-
H_f			H_f			-	-
H_g			H_g			-	-

35 mM $BPA4^+$			35 mM $BPA4^+/[Fe^{II}(CN)_6]^{4-}$			$(\delta_{obs} - \delta_{BPA4})$*/ppm*	$(\delta_{obs} - \delta_{BPA4})$/Hz[c]
H_{BPA4}	δ_{BPA4}/ppm[a]	J/Hz	H_{BPA4}	δ_{obs}/ppm[b]	J/Hz		
H_a	5.842	-	H_a	5.893	-	0.051	30.61
H_b	8.915	6.06	H_b	8.968	6.84	0.053	31.81
H_c	8.235	5.94	H_c	8.267	6.78	0.032	19.20
H_d	8.417	-	H_d	8.431	-	0.014	8.40
H_e	multiplicity 7.530 – 7.567		H_e	one broad signal 7.568		-	-
H_f			H_f			-	-
H_g			H_g			-	-

45 mM $BPA4^+$			45 mM $BPA4^+/[Fe^{II}(CN)_6]^{4-}$			$(\delta_{obs} - \delta_{BPA4})$/ppm	$(\delta_{obs} - \delta_{BPA4})$/Hz[c]
H_{BPA4}	δ_{BPA4}/ppm[a]	J/Hz	H_{BPA4}	δ_{obs}/ppm[b]	J/Hz		
H_a	5.849	-	H_a	5.912	-	0.063	37.81
H_b	8.920	6.90	H_b	8.993	6.84	0.073	43.81
H_c	8.243	6.84	H_c	8.288	6.78	0.045	27.01
H_d	8.424	-	H_d	8.449	-	0.025	15.00
H_e	multiplicity 7.533 – 7.579		H_e	one broad signal 7.623		-	-
H_f			H_f			-	-
H_g			H_g			-	-

[a] observed ^{1}H-NMR chemical shifts of pure AX solution ($X \equiv I^-$ for $PAM4^+$, and $X \equiv Cl^-$ for $BPA4^+$)

[b] observed ^{1}H-NMR chemical shifts of A^+ in equimolar $A^+/[Fe(CN)_6]^{4-}$ solution

[c] $(\delta_{obs} - \delta_{PAM4}) \cdot 600.13$ MHz

^{57}Fe Mössbauer spectra

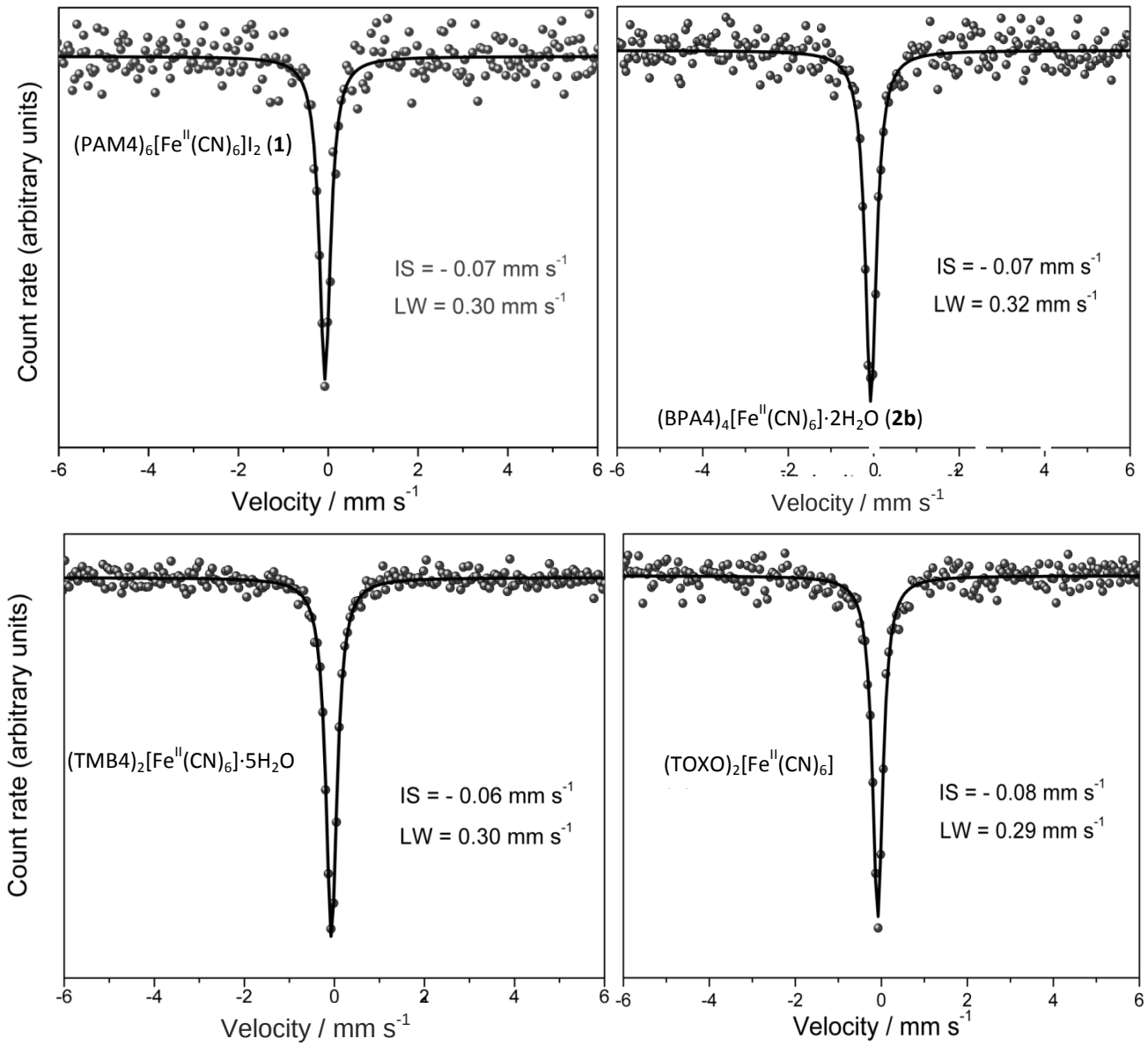

Fig. S6 ^{57}Fe Mössbauer spectra of the solid supramolecular complexes. Isomer shift (IS) and line width (LW) values relative to α-Fe at 298 K.

FTIR spectra

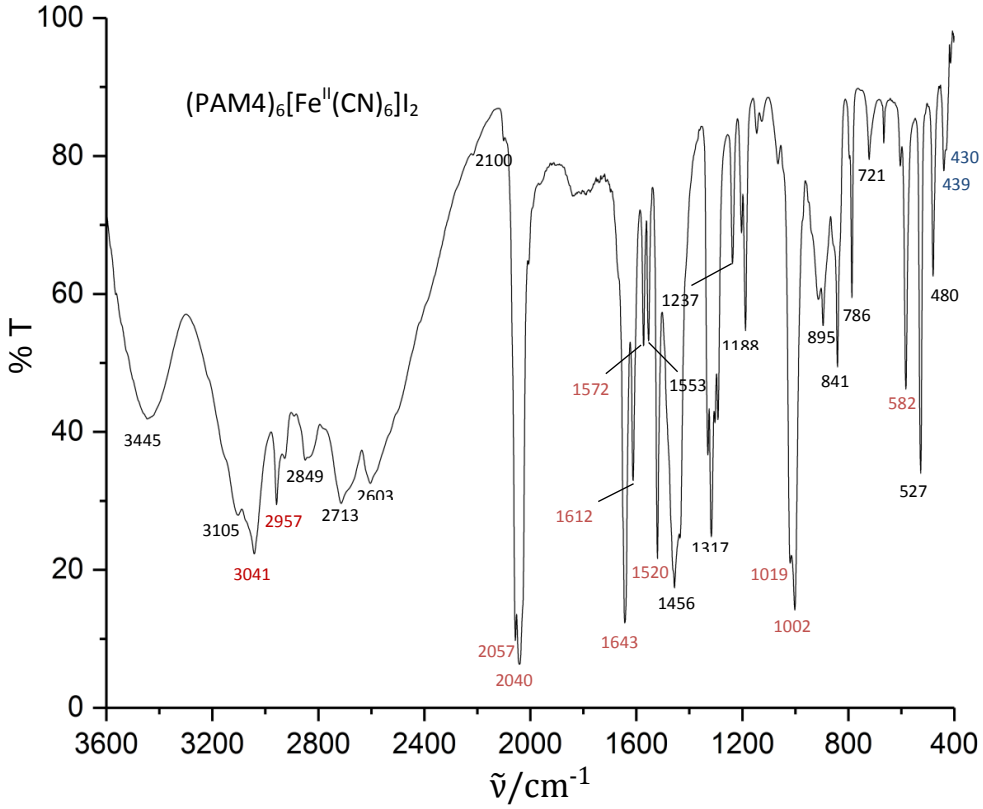

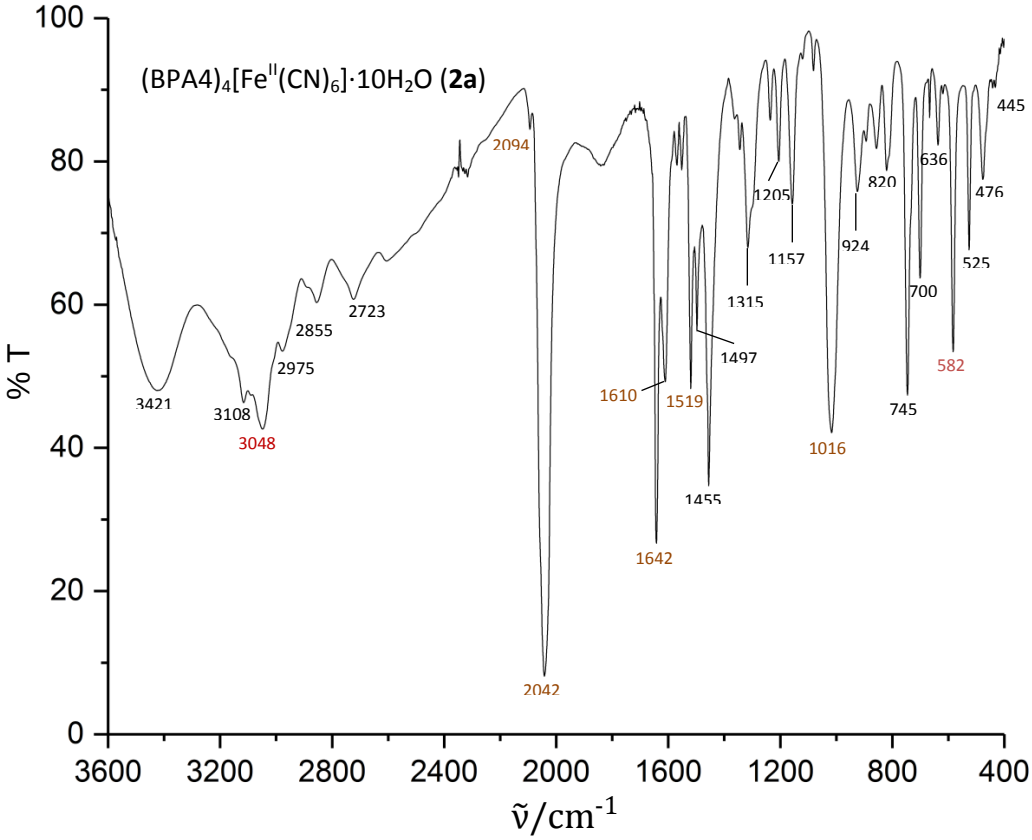

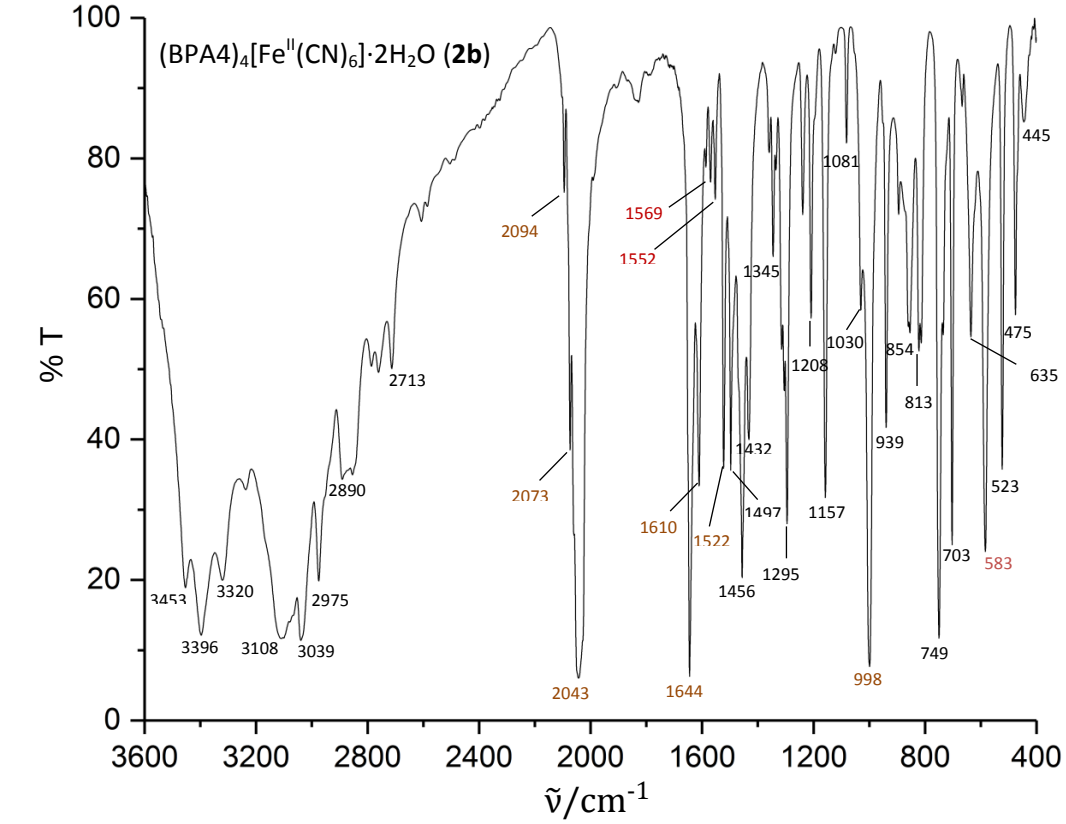
(BPA4)4[FeII(CN)6]·2H2O (2b)
% T
ṽ/cm-1
100
80
60
40
20
0
3600
3200
2800
2400
2000
1600
1200
800
400
3453
3396
3320
3108
3039
2975
2890
2713
2094
2073
2043
1644
1610
1569
1552
1522
1497
1456
1432
1345
1295
1208
1157
1081
1030
998
939
854
813
749
703
635
583
523
475
445

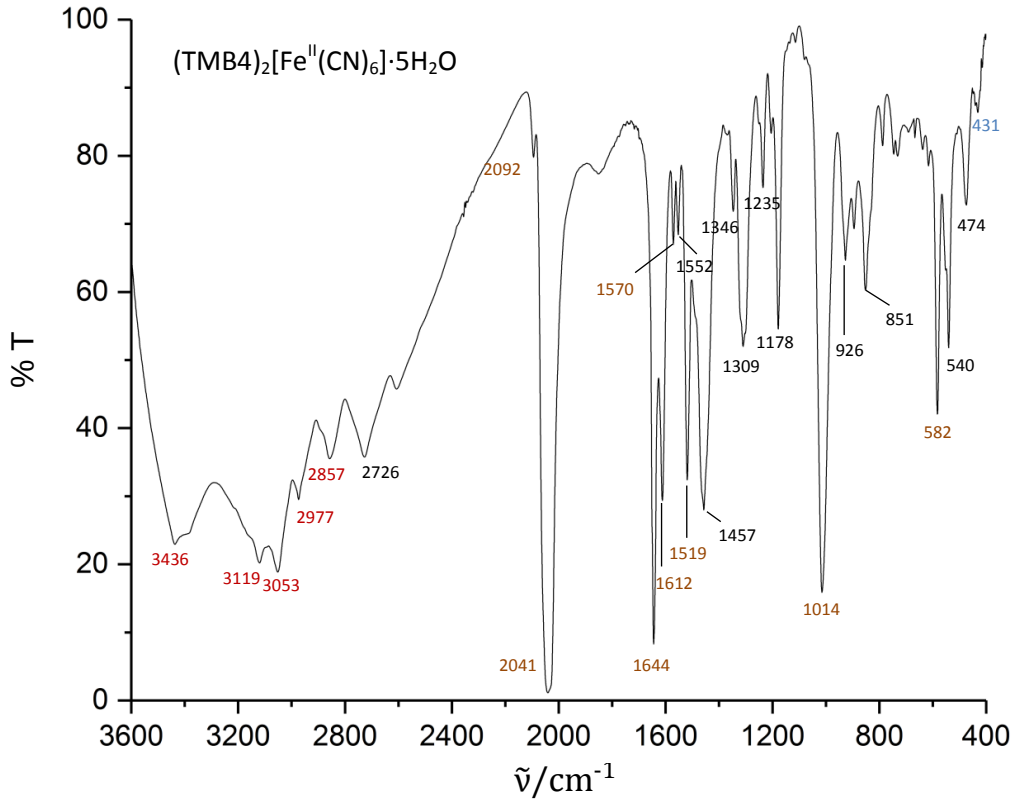
(TMB4)2[FeII(CN)6]·5H2O
% T
ṽ/cm-1
100
80
60
40
20
0
3600
3200
2800
2400
2000
1600
1200
800
400
3436
3119
3053
2977
2857
2726
2092
2041
1644
1612
1570
1552
1519
1457
1346
1309
1235
1178
1014
926
851
582
540
474
431

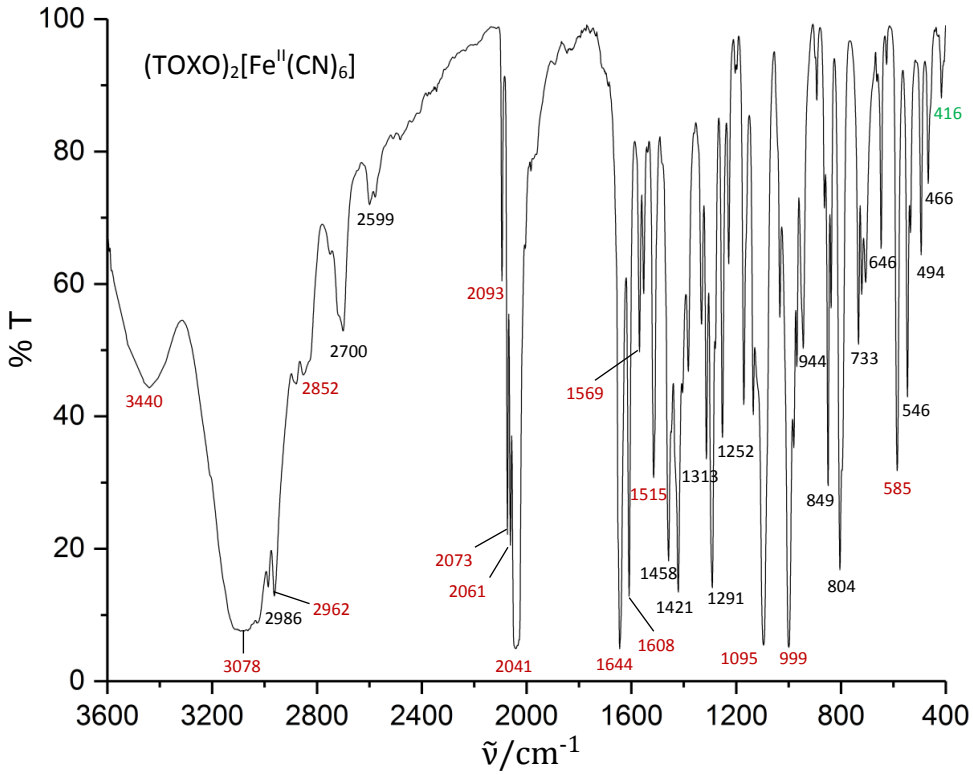

Fig. S7 FTIR spectra of the solid supramolecular complexes (KBr pellets) at 298 K.

DIFFUSE REFLECTANCE UV/VIS SPECTROSCOPIC ANALYSIS

The spectra of supramolecular solids in the range of 200 to 1000 nm were analyzed in comparison with the spectra of pure composites. Absorption spectra were constructed from diffuse reflectance measurements by expressing the apparent absorbance as log(1/*R*). The assignation of bands is presented in Table S3. The optical band gap (E_g) for the supramolecular complexes was determined as the intersection point between the energy axis and the line extrapolated from the linear portion of the absorption edge in a plot of of $(F(R)h\upsilon)^2$ against energy *E*. The Kubelka-Munk function, $F = (1 - R)^2/2R$, was converted from the recorded diffuse reflectance data, where *R* is the reflectance of an infinitely thick layer at a given wavelength.

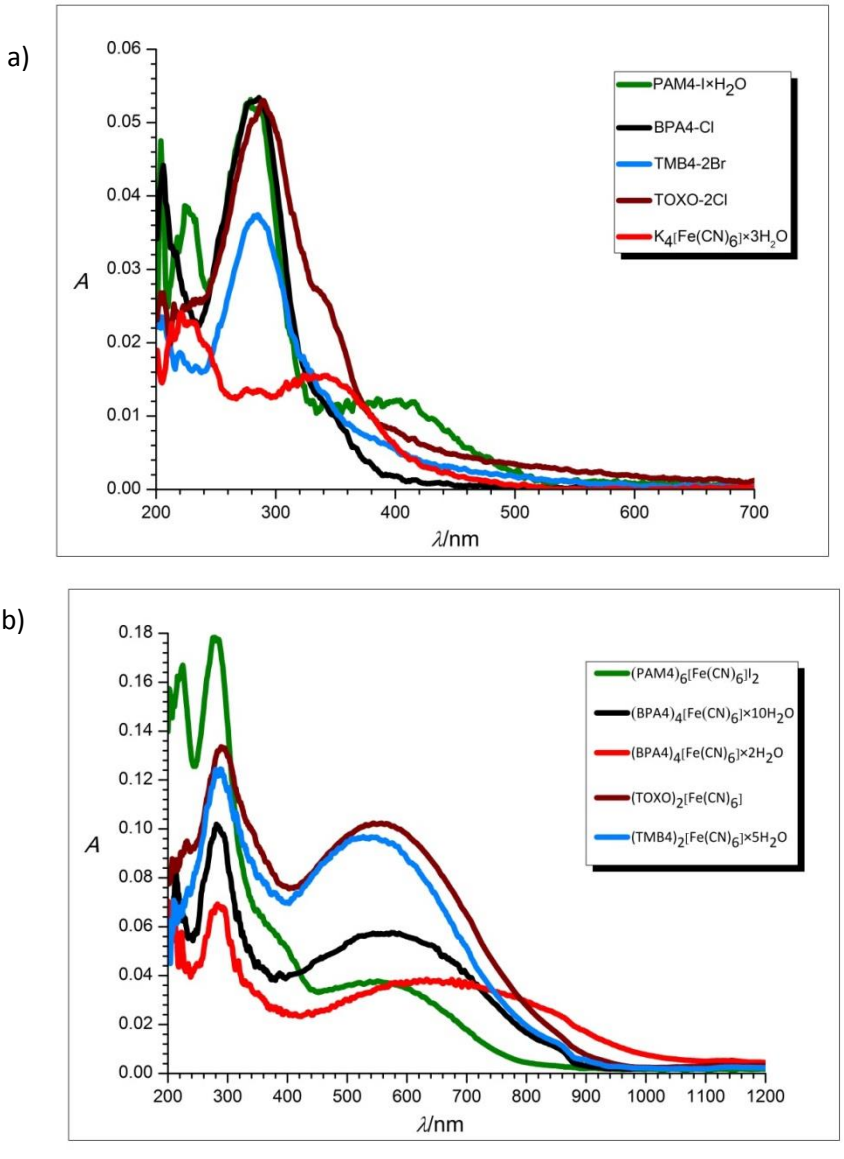

Fig. S8 Diffuse reflectance spectra of a) pyridinium-4-oxime halogenides and potasium hexacyanoferrate(II) trihydrate b) solid supramolecular complexes.

Table S3 Characteristic bands maxima in diffuse reflectance spectra and assignments.

Acceptor	λ_{max} **/nm**	**Assignation**
PAM4-I	205	$\pi_{oxime} \rightarrow \pi^*_{oxime}$
	225	$I(^3P_{3/2}) \rightarrow I(^3P_{3/2})^*$
	285	$\pi_{oxime} \rightarrow \pi^*_{oxime}$
	330-420 (br)	CT ($n_{5p\text{-}iodide} \rightarrow \pi^*_{oxime}$)
BPA4-Cl·H_2O	202	$\pi_{oxime} \rightarrow \pi^*_{oxime}$
	280	$\pi_{oxime} \rightarrow \pi^*_{oxime}$
	320-380 (sh)	CT ($n_{3p\text{-}chloride} \rightarrow \pi^*_{oxime}$)
TMB4-2Br	204	$\pi_{oxime} \rightarrow \pi^*_{oxime}$
	285	$\pi_{oxime} \rightarrow \pi^*_{oxime}$
TOXO-2Cl	203	$\pi_{oxime} \rightarrow \pi^*_{oxime}$
	280	$\pi_{oxime} \rightarrow \pi^*_{oxime}$
	330-380 (sh)	CT ($n_{3p\text{-}chloride} \rightarrow \pi^*_{oxime}$)
Donor		
$K_4[Fe(CN)_6] \cdot 3H_2O$	222	MLCT ($t_{2g} \rightarrow \pi_{CN}^*$)
	278	$d \rightarrow d^*$ ($t_{2g} \rightarrow t_{1u}^*$)
	332	$d \rightarrow d^*$ ($t_{2g} \rightarrow e_g^*$)
Complex		
$(PAM4)_6[Fe(CN)_6]I_2$	217	$I(^3P_{3/2}) \rightarrow I(^3P_{3/2})^*$ + MLCT ($t_{2g} \rightarrow \pi_{CN}^*$)
	276	$\pi_{oxime} \rightarrow \pi^*_{oxime}$ + $d \rightarrow d$ ($t_{2g} \rightarrow t_{1u}^*$)
	345-435 (sh)	CT ($n_{5p\text{-}iodide} \rightarrow \pi^*_{oxime}$) + $d \rightarrow d^*$ ($t_{2g} \rightarrow e_g^*$)
	554 (br)	IICT ($t_{2g} \rightarrow \pi^*_{oxime}$)
$(BPA4)_4[Fe(CN)_6] \cdot 10H_2O$	211	$\pi_{oxime} \rightarrow \pi^*_{oxime}$
	220	MLCT ($t_{2g} \rightarrow \pi_{CN}^*$)
	283	$\pi_{oxime} \rightarrow \pi^*_{oxime}$ + $d \rightarrow d^*$ ($t_{2g} \rightarrow t_{1u}^*$)
	563 (br)	IICT ($t_{2g} \rightarrow \pi^*_{oxime}$)
$(BPA4)_4[Fe(CN)_6] \cdot 2H_2O$	210	$\pi_{oxime} \rightarrow \pi^*_{oxime}$
	220	MLCT ($t_{2g} \rightarrow \pi_{CN}^*$)
	283	$\pi_{oxime} \rightarrow \pi^*_{oxime}$ + $d \rightarrow d^*$ ($t_{2g} \rightarrow t_{1u}^*$)
	645 (br)	IICT ($t_{2g} \rightarrow \pi^*_{oxime}$)
$(TMB4)_2[Fe(CN)_6] \cdot 5H_2O$	220	MLCT ($t_{2g} \rightarrow \pi_{CN}^*$)
	278	$\pi_{oxime} \rightarrow \pi^*_{oxime}$ + $d \rightarrow d^*$ ($t_{2g} \rightarrow t_{1u}^*$)
	535 (br)	IICT ($t_{2g} \rightarrow \pi^*_{oxime}$)
$(TOXO4)_2[Fe(CN)_6]$	207	$\pi_{oxime} \rightarrow \pi^*_{oxime}$
	230	MLCT ($t_{2g} \rightarrow \pi_{CN}^*$)
	285	$\pi_{oxime} \rightarrow \pi^*_{oxime}$ + $d \rightarrow d^*$ ($t_{2g} \rightarrow t_{1u}^*$)
	548 (br)	IICT ($t_{2g} \rightarrow \pi^*_{oxime}$)

CRYSTALLOGRAPHIC DATA

Table S4 The crystallographic data for **1** and **2a**.

	1	**2a**
Chemical formula	$C_{48}H_{54}FeI_2N_8O_6$	$C_{58}H_{72}FeN_{14}O_{14}$
Molecular weight (g mol^{-1})	1288.73	1245.14
Crystal colour, habit	red-brown, plate	red-brown, prism
Crystal size (mm^3)	0.09 × 0.25 × 0.30	0.11 × 0.25 × 0.26
Crystal system	triclinic	triclinic
Space group	*P* -1	*P* -1
Unit-cell parameters		
a (Å)	9.8846(6)	9.2150(5)
b (Å)	10.8052(6)	12.2553(5)
c (Å)	13.4619(7)	16.2052(8)
α (°)	99.573(4)	108.627(4)
β (°)	98.738(5)	95.042(4)
γ (°)	97.891(5)	105.537(4)
V (Å^3)	1381.69(14)	1640.43(15)
Z	2	2
D_{calc} (g cm^{-3})	1.549	1.260
T (K)	293(2)	293(2)
Radiation, *λ* (Å)	MoKα, 0.71073	MoKα, 0.71073
μ (mm^{-1})	1.454	0.301
ϑ range for data collection (°)	4.2 to 29.0	4.2–27.5
Ranges of indices	–13 ≤ *h* ≤ 11	–11 ≤ *h* ≤ 7
	–14 ≤ *k* ≤ 14	–11 ≤ *k* ≤15
	–17 ≤ *l* ≤ 18	–21 ≤ *l* ≤ 21
No. of collected data	14255	14585
No. of unique data, R_{int}	7309, 0.0293	7455, 0.0294
No. of observed data [$I \geq 2\sigma(I)$]	5057	6036
R_1, wR_2 [$I \geq 2\sigma(I)$]	0.0371, 0.0718	0.0563, 0.1410
R_1, wR_2 [all data]	0.0648, 0.0843	0.0724, 0.1534
S	1.009	0.997
Number of parameters	346	420
Min. and max. electron density (Å^{-3})	–0.37 and 0.66	–0.41 and 0.35
CCDC no.	1827974	1827975

Table S5 Selected bond lengths (Å) for **1** and **2a**.

bond	bond lengths	
	1	**2a**
Fe–C1	1.913(2)	1.898(2)
Fe–C2	1.923(3)	1.913(2)
Fe–C3	1.927(2)	1.9107(19)
C1–N1	1.156(3)	1.152(3)
C2–N2	1.153(3)	1.154(3)
C3–N3	1.148(3)	1.148(3)
CnA[a]–N2A	1.273(3)	1.261(3)
CnB[a]–N2B	1.267(3)	1.244(4)
C8C–N2C	1.268(2)	
N2A–O1A	1.371(2)	1.379(2)
N2B–O1B	1.379(2)	1.382(4)
N2C–O1C	1.380(2)	

[a] n = 8 for **1** and n = 14 for **2a**

Table S6 Hydrogen bonds (Å) and D–H···A angles (°) in **1** and **2a**.

D–H···A	D–H	H···A	D···A	D–H···A
		1		
O1A–H1A···N1^{i}	0.82	1.80	2.610(3)	171
O1B–H1B···N2^{ii}	0.82	1.85	2.662(3)	174
O1C–H1C···N3^{iii}	0.82	1.88	2.683(3)	166
C2A–H2A···N2	0.93	2.58	3.404(3)	148
C3A–H3A···O1B^{iv}	0.93	2.57	3.153(3)	121
C6A–H6A···I^{i}	0.93	2.98	3.592(2)	125
C6C–H6C···I	0.93	2.98	3.634(3)	128
		2a		
O1A–H1A···N1^{v}	0.82	1.78	2.589(3)	167
O1B–H1B···Ow5^{vi}	0.82	1.73	2.546(4)	174
Ow1–H11···N2	0.85	1.90	2.748(4)	172
Ow1–H12···O1a^{vii}	0.85	1.93	2.786(3)	177
Ow2–H21···Ow1^{viii}	0.85	1.92	2.764(4)	170
Ow3–H31···N1^{i}	0.85	2.47	3.189(5)	143
Ow4–H41···Ow3^{i}	0.85	1.89	2.727(5)	170
Ow4–H42···Ow1^{viii}	0.85	1.99	2.775(4)	153
Ow5–H51···N3^{i}	0.85	1.89	2.722(4)	165
Ow5–H52···Ow4^{ix}	0.85	1.88	2.691(5)	160
C3B–H3B···N3^{i}	0.93	2.47	3.258(5)	143
C5A–H5A···N3^{x}	0.93	2.54	3.356(3)	146
C5B–H5B···Ow2^{xi}	0.93	2.42	3.345(4)	172
C7B–H37B···N1^{i}	0.97	2.60	3.546(5)	165
Ow2–H22···N2B^{xii}	0.85	2.32	3.085(4)	149

Symmetry operators: (i) 1-x,1-y,1-z; (ii) 1+x,y,1+z; (iii) 1-x,-y,-z; (iv) -1+x,y,-1+z; (v) 1-x,2-y,1-z; (vi) 2-x,1-y,-z; (vii) x, –1+ y,z; (viii) x,1+y,z; (ix) 1 + x, y, z; (x) -x,1-y,1-z; (xi) 1-x,1-y,-z; (xii) -x+1, -y+2, -z+2.

a) b)

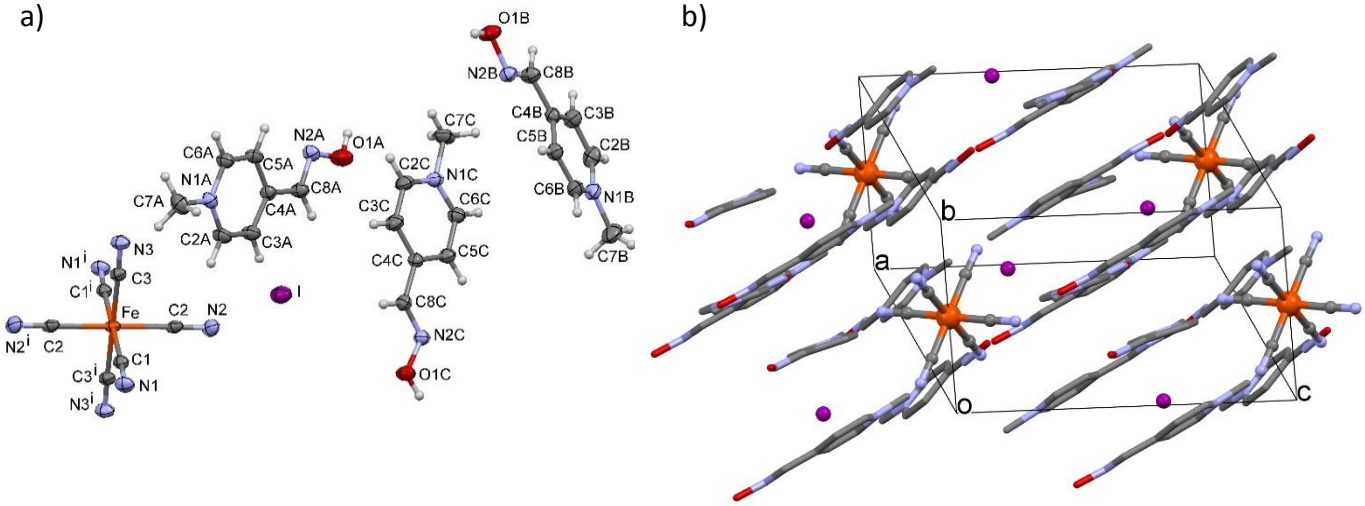

Fig. S9 a) Drawing of the $[Fe^{II}(CN)_6]^{4-}$, I^- and three $PAM4^+$ cations in **1** with the atom labeling scheme. Ellipsoids are at the 40% probability level. Symmetry code: (i) -x, 1-y, -z.; b) packing of **1** in the unit cell.

a) b)

Fig. S10 a) Crystals of **1a** and b) schematic drawing of the crystal used for data collection with face indices.

a)

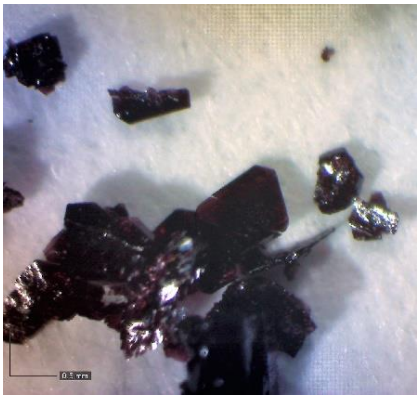

b)

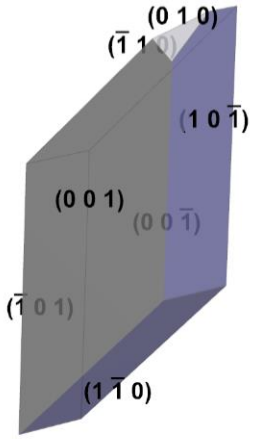

Fig. S11 a) Crystals of **2a** and b) schematic drawing of the crystal used for data collection with face indices.

THERMOGRAVIMETRIC AND DIFFERENTIAL THERMAL ANALYSIS

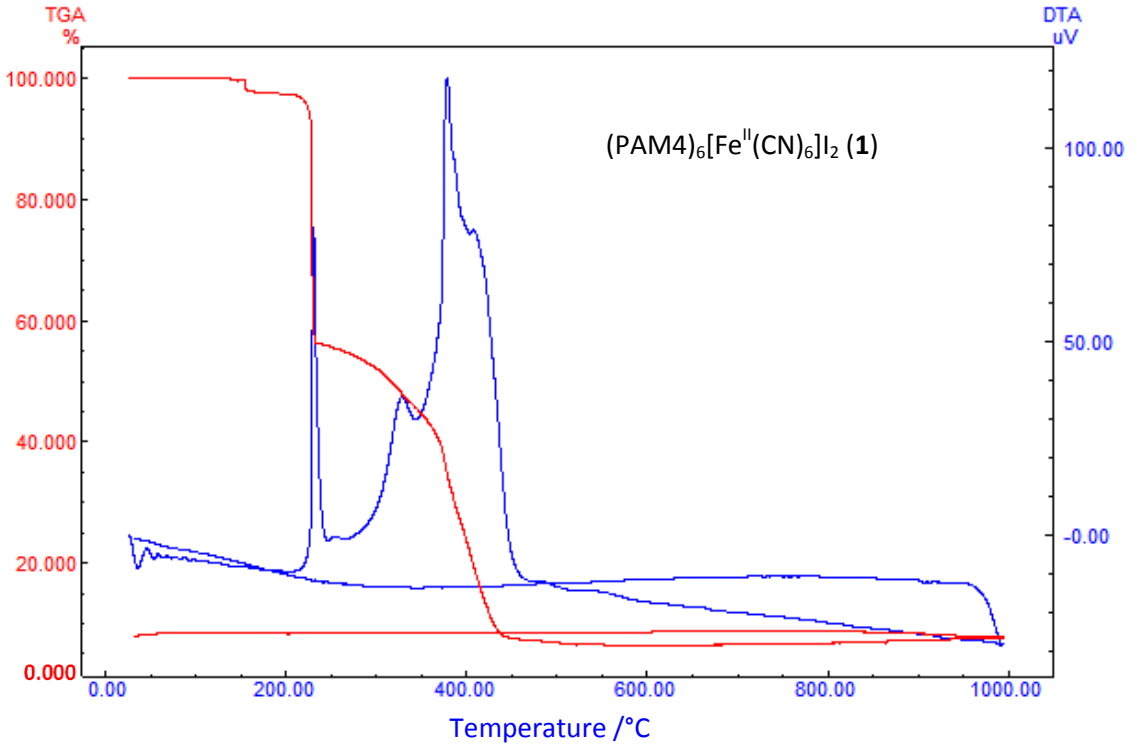

$(PAM4)_6[Fe^{II}(CN)_6]I_2$ (**1**)

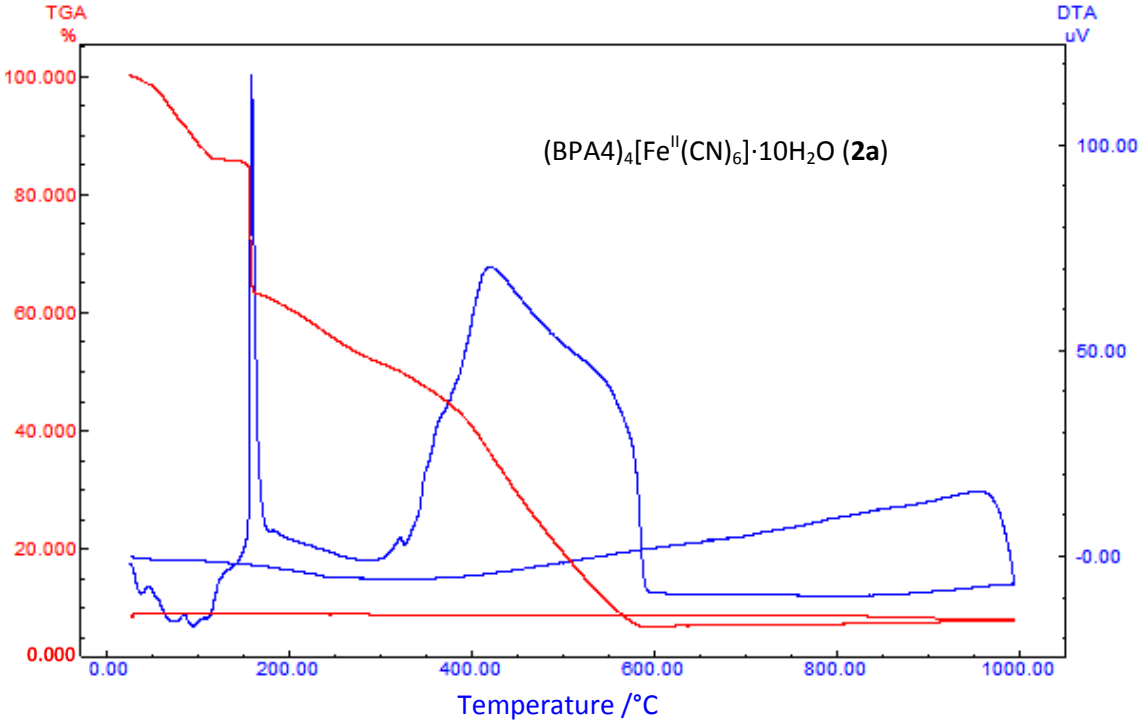

$(BPA4)_4[Fe^{II}(CN)_6]\cdot 10H_2O$ (**2a**)

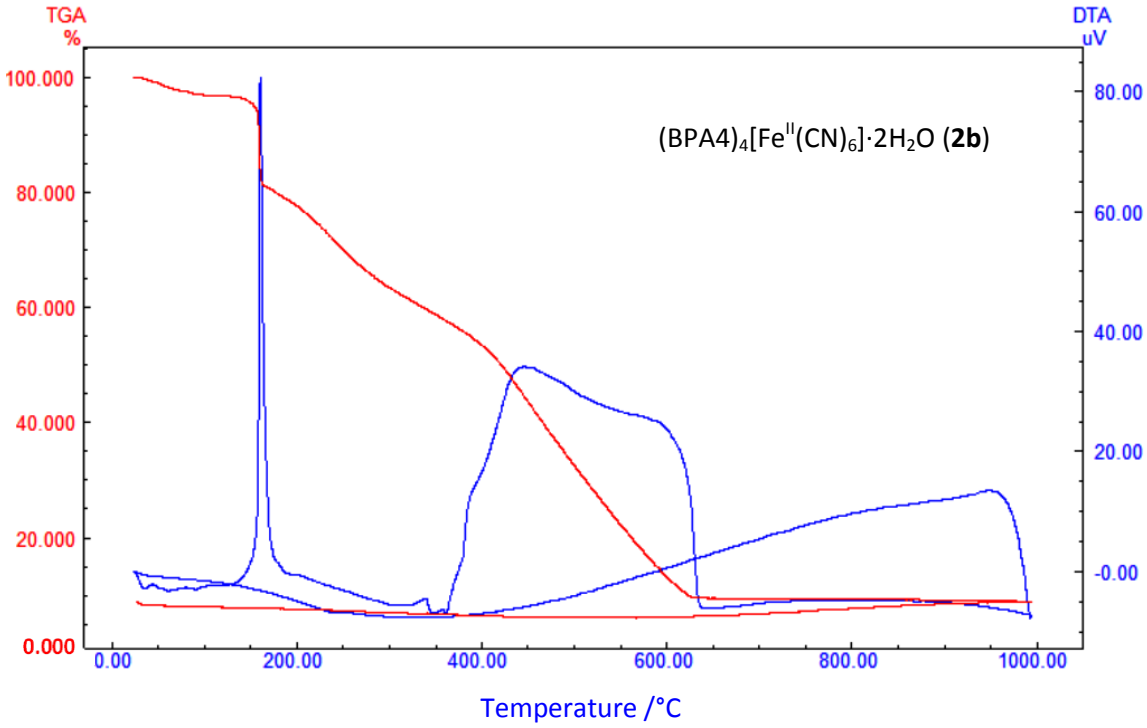
TGA
%
DTA
uV
100.000
80.000
60.000
40.000
20.000
0.000
80.00
60.00
40.00
20.00
-0.00
0.00
200.00
400.00
600.00
800.00
1000.00
(BPA4)4[Fe^II(CN)6]·2H2O (2b)
Temperature /°C

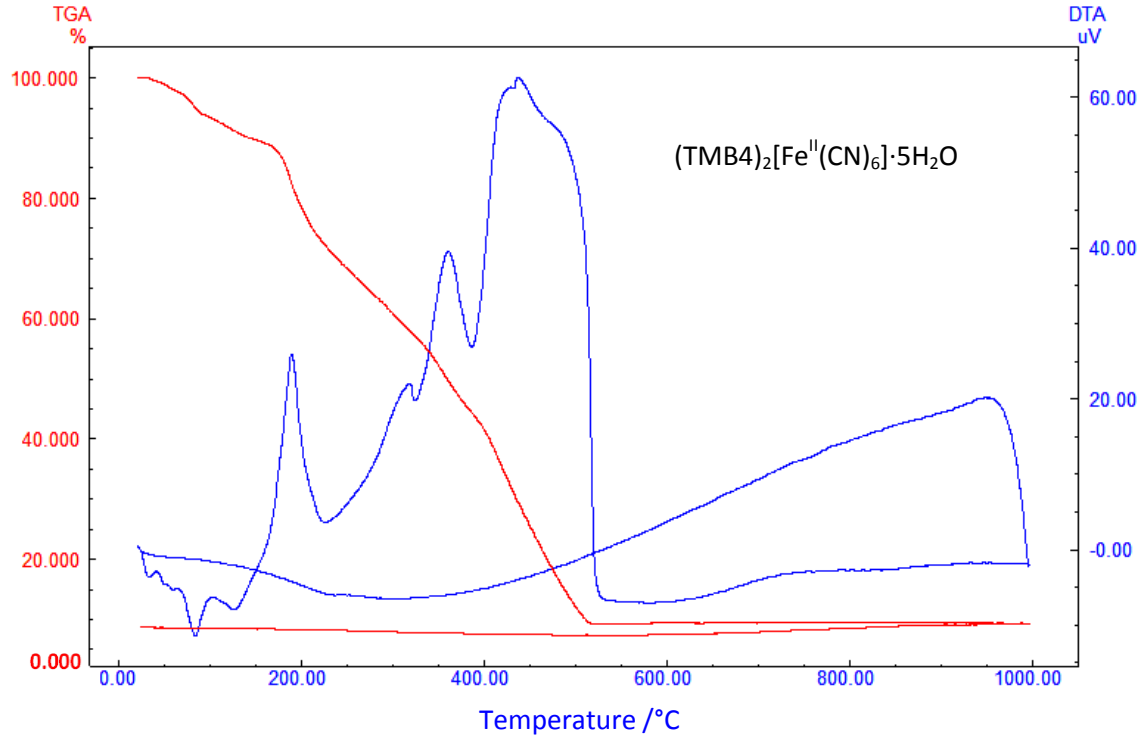
TGA
%
DTA
uV
100.000
80.000
60.000
40.000
20.000
0.000
60.00
40.00
20.00
-0.00
0.00
200.00
400.00
600.00
800.00
1000.00
(TMB4)2[Fe^II(CN)6]·5H2O
Temperature /°C

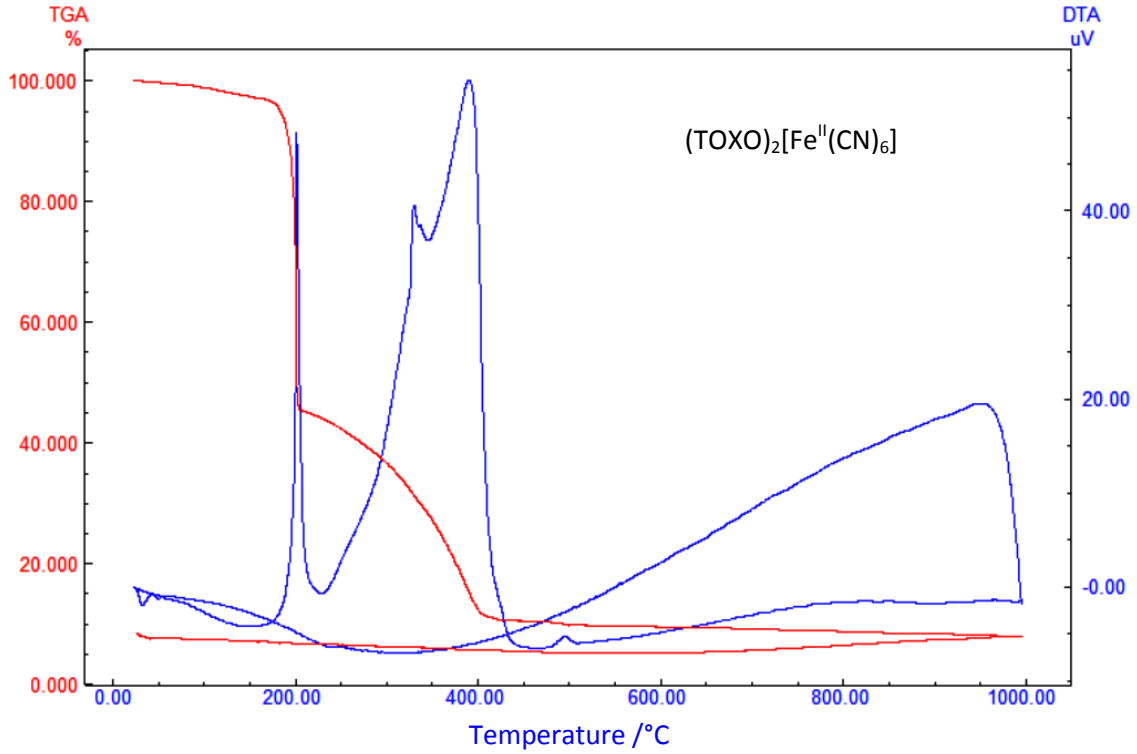

Fig. S12 TG and DTA curves of the solid supramolecular complexes.